Pergamon

Int. J. Heat Mass Transfer. Vol. 40, No. 5, pp. 993–1000, 1997

0017–9310/97 $17.00 + 0.00

PII: S0017–9310(96)00197–4

Optimum plate separation in vertical parallel-plate channels for natural convective flows: incorporation of large spaces at the channel extremes

BIAGIO MORRONE
DETEC, Universitá degli Studi Federico II, Piazzale Tecchio 80, 80125 Naples, Italy

ANTONIO CAMPO
Nuclear Engineering Department, Idaho State University, Pocatello, ID 83209, U.S.A.

and

ORONZIO MANCA†‡
DETEC, Universitá degli Studi Federico II, Piazzale Tecchio 80, 80125 Naples, Italy

(*Received* 1 *August* 1995 *and in final form* 6 *June* 1996)

Abstract—This paper addresses the problem of optimizing the plate separation of an open, parallel-plate channel that is cooled by natural convection air flow. The plates are symmetrically heated by uniform heat flux. The I-shaped computational domain comprised two subdomains: the actual physical domain between the plates, and two large rectangular reservoirs placed upstream of the entrance and downstream of the exit. The aggregate subdomains accommodated the diffusion phenomena by momentum and energy that occur outside the channel. The full elliptic Navier–Stokes and energy equations are solved numerically in the composite domain. Correlations of the optimal values of the plate spacing as a function of the Gr_L number and of the induced mass flow rate, as well as thermal and velocity profiles, are presented for air.

1. INTRODUCTION

Packaging of electronic components poses severe demands and constraints for their efficient cooling and of course necessitates detailed knowledge of the optimization of the heat dissipation by natural convection inside vertical, parallel-plate channels.

Bar-Cohen and Rohsenow [1] developed a Churchill-type correlation equation for the natural convective heat transfer coefficient covering the two asymptotes, one for a fully developed channel regime and the other for a single plate boundary layer regime. Previous knowledge of the natural convective heat transfer coefficient for each asymptote was indispensable. An optimum plate-to-plate spacing, b/L, was then extracted from the composite correlation equation by maximizing the total heat dissipation through the channel. Anand *et al.* [2] determined the optimal spacing b/L numerically by calculating the flow and temperature distribution based on a finite-difference solution to the parabolic version of the conservation equations. These authors utilized a computational domain that coincided with the physical domain in conformity with the adopted model. Due to the parabolic nature of the equations, diffusion phenomena by both momentum and energy that occur outside of the channel were excluded. Also, the aspect ratio b/L was made an independent parameter by defining a Grashof number in terms of the channel length L. In contrast with the work by Bar-Cohen and Rohsenow [1], knowledge of the natural convective heat transfer coefficient was not known *a priori* and obviously it emerged naturally as a by-product of the calculation procedure. For completeness, it should be added that Bodoia and Osterle [3] and Levy [4] did some preliminary calculations, conducive to the estimation of optimum spacings between vertical channels with limited success.

From a historical standpoint, the first investigation on natural convection flows through heated vertical, parallel-plate channels combining the full elliptic character of the conservation equations with the enlarged computational domains are those of Kettle-

† Author to whom correspondence should be addressed.
‡ Present address: Dipartimento di Ingegneria, Aerospazale, Seconde Università degli Studi di Napoli, Via Roma 29, 81031 Aversa (CE), Italy.

NOMENCLATURE

a	thermal diffusivity [$m^2 s^{-1}$]
b	channel gap [m]
g	gravity acceleration [$m s^{-2}$]
Gr_b	Grashof number, equation (1)
Gr_L	Grashof number, equation (9)
h_X	local convective coefficient [$W m^{-2} K^{-1}$]
k	thermal conductivity [$W m^{-1} K^{-1}$]
L	channel height [m]
L_X	height of the reservoir [m]
L_Y	width of the reservoir [m]
Nu_X	local Nusselt number, equation (6)
Nu_b	mean Nusselt number, equation (7)
Nu_L	mean Nusselt number, equation (8)
p	pressure [Pa]
P	dimensionless pressure, equation (1)
Pr	Prandtl number
q_w	wall heat flux [$W m^{-2}$]
t	time [s]
u, v	velocity components along x-, y-directions [$m s^{-1}$]
U, V	dimensionless velocities, equation (1)
x, y	Cartesian coordinates, Fig. 1 [m]
X, Y	dimensionless coordinates.

Greek symbols

β	volumetric coefficient of expansion [K^{-1}]
Δ	difference between two values
ε	convergence criterion
η	dummy variable
ν	kinematic viscosity [$m^2 s^{-1}$]
ψ	stream function [$m^2 s^{-1}$]
Ψ	dimensionless stream function, equation (1)
ϕ	dimensionless temperature, equation (1)
ρ	density [$kg m^{-3}$]
σ	relaxation parameter (SOR)
τ	dimensionless time, equation (1)
ω	vorticity [s^{-1}]
Ω	dimenionless vorticity, equation (1).

Subscripts

∞	free stream condition
b	refers to the channel gap
L	refers to the channel height
opt	optimal value
w	wall
w_1	left wall
w_2	right wall.

borough [5] and Nakamura *et al.* [6]. Recently several studies by Chang and Lin [7], Naylor *et al.* [8], Martin *et al.* [9], Shyy *et al.* [10] and Manca *et al.* [11] have elaborated on this kind of combined mathematical model/computational domain using computer intensive calculations and sophisticated equipment.

Despite the fact that the above-cited references have stressed the paramount importance of the realistic elliptic model vs the idealistic parabolic model for the conservation equations attached to extended computational domains, none of them examined aspects associated with the optimization of the plate spacing and the maximization of the total heat transfer. This single aspect constitutes the central motivation for undertaking this project with a particular emphasis on air flows applied to electronic cooling. Accordingly, an elliptic model was preferred here, to analyze the heat and air flow inside a vertical channel under the action of symmetric heating. The computational domain comprised the actual physical domain between the two channel plates, as well as two relatively large domains placed upstream of the channel entrance and downstream of the channel exit. These I-type composite domains resemble open, unbounded spaces that serve to accommodate the diffusion phenomena by both momentum and energy that could occur outside of the channel. Using a finite-difference discretization technique, the system of conservation equations has been solved numerically providing the velocity, pressure and temperature fields of the air medium. The computed results have been post-processed and analyzed from an optimization perspective. The optimum spacing, $(b/L)_{opt}$, has been presented in graphical form as a function of the Grashof numbers, Gr_L, for a fixed $Pr = 0.71$, and a correlation between the same variables has been proposed. Further, a correlation between the dimensionless mass flow rate and the thermo-geometrical parameters involved in the analysis, i.e. Gr_L and b/L, has been presented.

2. DESCRIPTIVE EQUATIONS

A vertical, parallel-plate channel where both plates are equally heated with uniform flux q_w is depicted in Fig. 1(a). The imbalance between the temperature of the ambient air T_∞, and the temperature of the heated plates draws a mass of fluid into the vertical channel. The dimensionalization process of the variables relies on:

$$X = \frac{x}{b} \quad Y = \frac{y}{b} \quad \tau = \frac{tv}{b^2}$$

$$U = \frac{ub}{v} \quad V = \frac{vb}{v} \quad P = \frac{(p - p_\infty)b^2}{\rho v^2}$$

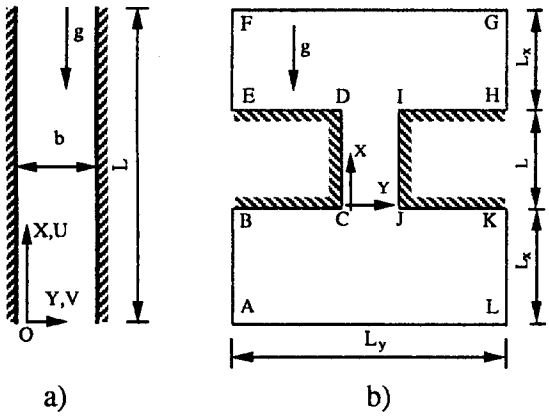

Fig. 1. Sketch of the system: (a) physical domain; (b) computational domain.

$$\Psi = \frac{\psi}{\nu} \quad \Omega = \frac{\omega}{\nu b^2} \quad \phi = \frac{k(T-T_\infty)}{q_w b}$$

$$Gr_b = \frac{g\beta q_w b^4}{k\nu^2} \quad Pr = \frac{\nu}{a} \tag{1}$$

permitting one to write the 2-D Navier–Stokes and energy equations as

$$\frac{\partial\Omega}{\partial\tau} + \frac{\partial(U\Omega)}{\partial X} + \frac{\partial(V\Omega)}{\partial Y} = \nabla^2\Omega - Gr_b\frac{\partial\phi}{\partial Y} \tag{2}$$

$$\frac{\partial^2\Psi}{\partial X^2} + \frac{\partial^2\Psi}{\partial Y^2} = -\Omega \tag{3}$$

$$\frac{\partial\phi}{\partial\tau} + \frac{\partial(U\phi)}{\partial X} + \frac{\partial(V\phi)}{\partial Y} = \nabla^2\phi. \tag{4}$$

As is customary, the physical properties of the fluid are taken as averaged over temperature range of operation, with the exception of the density in the buoyancy term, to comply with the Boussinesq approximation.

The imposed boundary conditions, rewritten of course in terms of stream function and vorticity, with reference to the Fig. 1(b), are:

$$\frac{\partial\Psi}{\partial Y} = 0 \quad \frac{\partial\Omega}{\partial Y} = 0 \quad \phi = 0 \quad \text{at AB and KL}$$

$$\frac{\partial\Psi}{\partial X} = 0 \quad \frac{\partial\Omega}{\partial X} = 0 \quad \phi = 0 \quad \text{at AL}$$

$$\Psi = \Psi_{w1} \quad \frac{\partial\Psi}{\partial X} = 0 \quad \frac{\partial\phi}{\partial X} = 0 \quad \text{at BC and DE}$$

$$\Psi = \Psi_{w1} \quad \frac{\partial\Psi}{\partial Y} = 0 \quad \frac{\partial\phi}{\partial Y} = -1 \quad \text{at CD}$$

$$\Psi = \Psi_{w2} \quad \frac{\partial\Psi}{\partial Y} = 0 \quad \frac{\partial\phi}{\partial Y} = 1 \quad \text{at IJ}$$

$$\frac{\partial^2\Psi}{\partial Y^2} = 0 \quad \frac{\partial\Omega}{\partial Y} = 0 \quad \frac{\partial\phi}{\partial Y} = 0 \quad \text{at EF and GH}$$

$$\Psi = \Psi_{w2} \quad \frac{\partial\Psi}{\partial X} = 0 \quad \frac{\partial\phi}{\partial X} = 0 \quad \text{at HI and JK}$$

$$\frac{\partial^2\Psi}{\partial X^2} = 0 \quad \frac{\partial\Omega}{\partial X} = 0 \quad \frac{\partial\phi}{\partial X} = 0 \quad \text{at FG.} \tag{5}$$

The local convective coefficient can be computed from the local Nusselt number

$$Nu_X = \frac{h_X b}{k} = \frac{1}{\phi_w}. \tag{6}$$

From here, two mean Nusselt numbers can be defined. One based on the plate separation, b:

$$Nu_b = \frac{\bar{h}b}{k} = \frac{b}{L}\int_0^{L/b} Nu_X\,dX \tag{7}$$

and the other based on the channel height, L:

$$Nu_L = \frac{\bar{h}L}{k} = \frac{L}{b}Nu_b \tag{8}$$

and a Grashof number based on the plate height L defined as:

$$Gr_L = Gr_b\frac{L^4}{b^4}. \tag{9}$$

3. NUMERICAL SCHEME

The numerical computation has been carried out by means of the finite-difference method, using the control volume approach.

The vorticity and energy equations (2), (4) were solved by the alternating-direction implicit (ADI) method. This method transforms the discretized PDEs into a tridiagonal, linear system of algebraic equations that can be easily solved by the Thomas algorithm. Further, the second upwind scheme (see ref. [12]) has been employed to discretize the convective derivatives, while for the diffusive derivatives a classical three-point central scheme has been adopted. The convective terms were linearized following the iterative procedure suggested by Roache [13]. The stream function has been determined by the successive line over-relaxation (SLOR) method involving an optimum relaxation factor σ of about 1.7. Once the equations of vorticity, stream function and energy are solved, then the convergence patterns for the time step have to be checked. Thus, the following convergence criterion chosen for steady-state

$$\left|\frac{\eta_{i,j}^{n+1} - \eta_{i,j}^{n}}{\eta_{i,j}^{n+1}}\right|_{\max} < \varepsilon \tag{10}$$

has to be verified at every (i,j) node, where η represents Ω or ϕ and ε was set equal to 10^{-5}. The computational procedure can be implemented by guessing an initial value for the stream function ψ_{w2}, at the right solid wall 2, together with $\psi_{w1} = 0$ at the left

solid wall 1. Thus, under these circumstances a forced convection flow with a reasonable mass flow rate is initially imposed. The selected value of the mass flow rate accounting for its limiting steady-state value is verified on a global basis by integrating the momentum equation along the centerline of the channel once the steady-state condition is attained.

For confined natural convection flows, far away from the entrance and exit of the channel, the pressure must be equal to that of the undisturbed environment. Then, for the chosen reduced computational domain the pressure relation

$$\Delta P = P(L_X + L) - P(-L_X) = 0 \qquad (11)$$

holds. Of course, this equality is translated into an inequality. In the latter, the second member, rewritten as ε is set equal to 5×10^{-2}. If the guessed value ψ_{w2} does not satisfy the equation (11), then a new value of ψ_{w2} is selected and the procedure repeated again, until equation (11) holds.

As far as the sensitivity of the grid is concerned, it depends on two components: the number of nodes and the dimensions of the reservoirs. Bearing this in mind, preliminary calculations have been carried out to ensure grid independency of the solution. After carefully testing several combinations of nodes in the grid, it was concluded that either 31×31 or 31×25 grid nodes inside the channel have to be employed to satisfy accuracy requirements. Also, these grids guaranteed a global energy balance inside the channel with an accuracy not greater than 0.5%.

Similar numerical experiments have been performed to estimate the minimum vertical and horizontal sizes of the reservoirs which do not affect the velocity, pressure and temperature fields inside the channel with an approximation of not more than 10^{-4}. Fixing the fluid to air ($Pr = 0.71$) and depending on the Grashof number and the aspect ratio selected, the dimensions L_X and L_Y range from 2.0 to 4.0 and 7.0 to 9.0, respectively.

The numerical procedure was first tested in ref. [11] and its outcome when compared with other numerical and experimental results, produced satisfactory agreement.

4. RESULTS AND DISCUSSION

In the following paragraph the results are presented for air as working fluid ($Pr = 0.71$). The analysis has been carried out for a range of Gr_L spanning between 10^2 and 10^5.

Figure 2 displays the variation of the local Nusselt numbers with the axial coordinate X parametrized by the aspect ratio, b/L, at two meaningful values of Gr_L, in the range investigated in this study. It can be noticed in both the figures that the family of local Nusselt numbers, Nu_X, exhibit their characteristic monotonic decreasing behavior with X. It is important to recognize that Nu_X does not begin with a infinite value at the channel inlet, $X = 0$. Instead, they begin with a realistic finite value due to the elliptic model chosen. The boundary layer approximation of the conservation equations impedes the utilization of the field variables in an appropriate way at the inlet region. The physical model adopted in this study takes into account the momentum and thermal diffusion in the axial direction; these effects can be appreciated at the channel entrance and even at the channel exit.

The areas below the local Nusselt number curves for each b/L value, are the mean Nusselt number defined in equation (8). It can be pointed out that as b/L increases the curves tend to move upward because of an increment in the nondimensional induced mass flow rate, as can be noticed in Fig. 3. This figure illustrates the dimensionless mass flow rate as a function of the aspect ratio, b/L, for different Grashof number values. The increase in the induced mass flow rate is caused by two effects: the growth of the cross-sectional area of the channel, viz. b, and the increase of the mean velocity of the fluid entering the channel. These two combined effects do not necessarily imply an increase in the mean dimensional velocities inside the channel. Thus, for all Gr_L numbers examined the area under the curves shown in Fig. 2 is magnified up to a fixed value of b/L.

A correlation between the dimensionless flow rate and the thermo-geometrical parameters involved in this study, i.e. Gr_L and b/L, has been obtained. The correlation, that holds in the range $10^2 \leqslant Gr_L \leqslant 10^5$

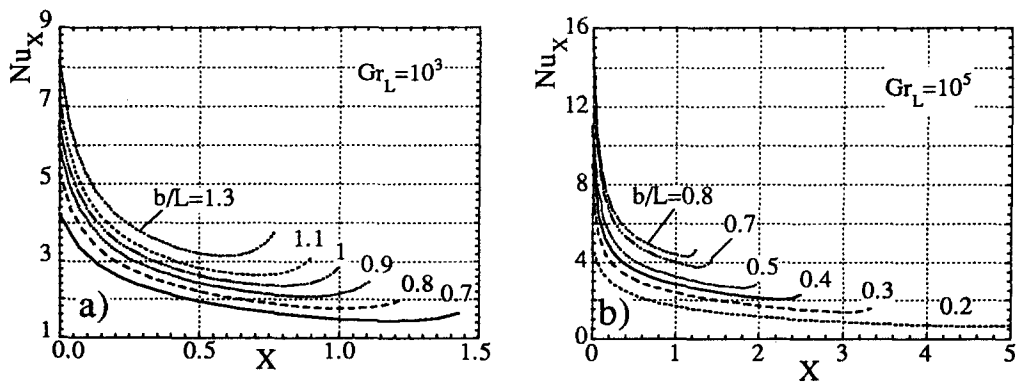

Fig. 2. Axial variation of the local Nusselt number at two Gr_L numbers and for several aspect ratios.

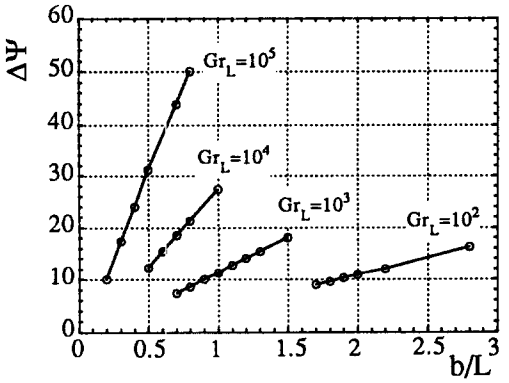

Fig. 3. Dimensionless induced mass flow rate vs aspect ratio, at different Gr_L.

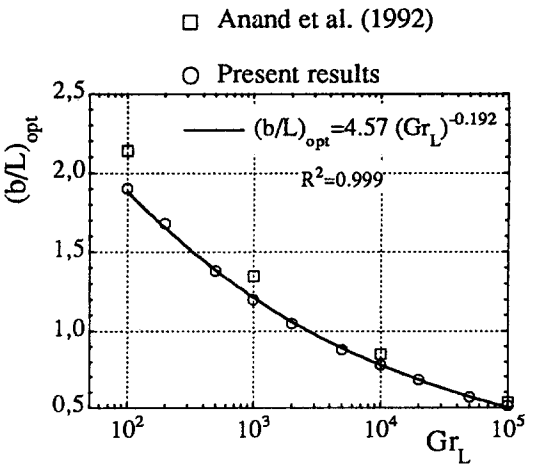

Fig. 5. Optimal aspect ratio b/L as a function of the Gr_L number compared to the results of Anand *et al.* [2].

and $0.2 \leqslant b/L \leqslant 3.0$, with a regression coefficient $R^2 = 0.993$, is:

$$\Delta\Psi = 0.810 \cdot (Gr_L)^{0.384} \cdot (b/L)^{1.17}. \qquad (12)$$

In accordance with the findings of Bar-Cohen and Rohsenow [1] and Anand *et al.* [2], optimal values of the aspect ratio, b/L, that render maximum the values of the mean Nusselt number, equation (8), can be computed. Figure 4 shows, in a sequential manner, the behavior of the mean Nusselt number, Nu_L, as a function of the aspect ratio b/L for the four Gr_L investigated in this paper. The associated optimal values of b/L, for which the mean Nu_L is maximum, can be easily inferred from these figures. As b/L decreases from infinity, that corresponds to the single-plate limit, up to a fixed value, there is an increasing 'chimney effect', that draws more fluid into the channel. The pressure drops, that will be shown in Fig. 6, increase as b/L decreases, due to the increasing induced flow rate and to the narrowing of the channel gap, b, for fixed height L. An optimum balance between the increasing pressure drops and the increasing 'chimney effect' gives rise to the optimum value of b/L, for each value of Gr_L. Moreover, the thermal field attains the fully developed condition for which the mean Nusselt number decreases. In addition, it can be realized that for large values of the aspect ratio b/L,

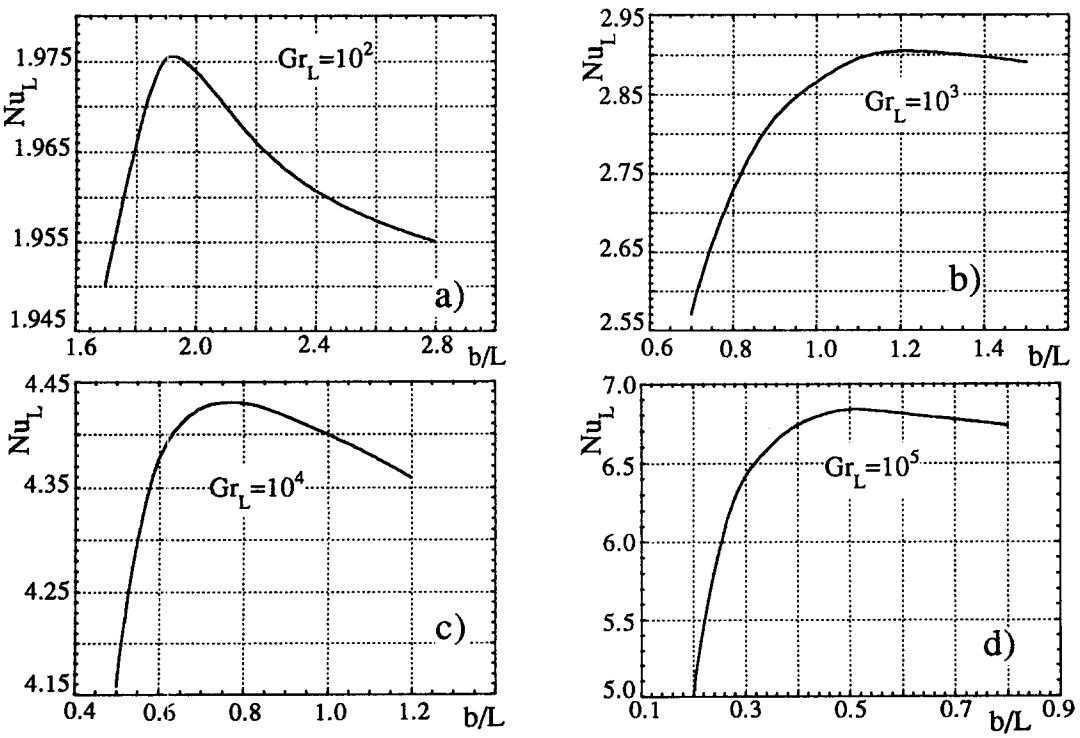

Fig. 4. Mean Nusselt number vs aspect ratio: (a) $Gr_L = 10^2$; (b) $Gr_L = 10^3$; (c) $Gr_L = 10^4$; (d) $Gr_L = 10^5$.

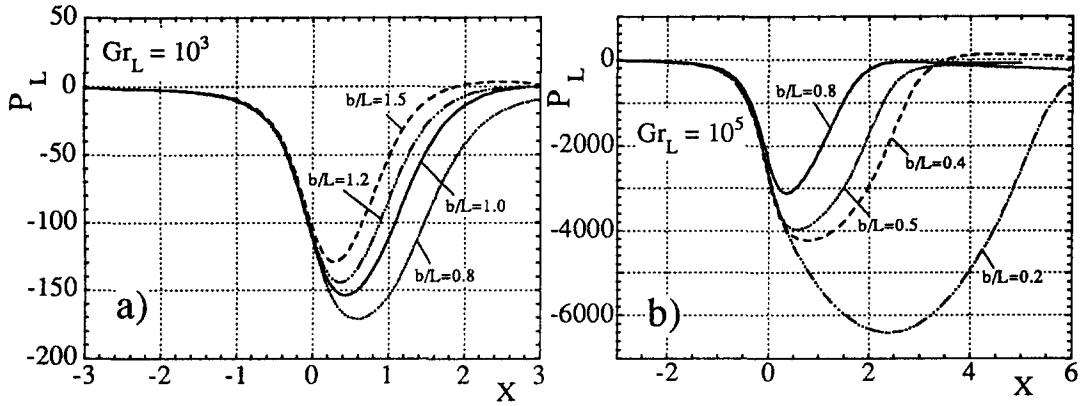

Fig. 6. Axial variation of the modified non-dimensional pressure along the centerline of the computational domain, at two Gr_L numbers and for several aspect ratios.

the mean Nusselt number tends to ones characterizing single-plate behaviour.

Figure 5 and Table 1 have been prepared concurrently with the objective of displaying the optimal aspect ratio $(b/L)_{opt}$ as a function of the Grashof number, Gr_L, separately. These qualitative results indeed constitute the backbone of this investigation. The results obtained from several runs have been fitted by a correlation between the $(b/L)_{opt}$ and the Gr_L with a regression coefficient $R^2 = 0.999$:

$$(b/L)_{opt} = 4.57 \cdot (Gr_L)^{-0.192}. \quad (13)$$

In the same figure the optimal values obtained in [2] are included for comparison purposes and the discrepancy between the two data sets is evident. For all Gr_L, the optimal aspect ratios $(b/L)_{opt}$ computed in [2] overpredict the present results consistently. The order of magnitude of the relative errors is around 10%. Actually, from the standpoint of packaging of electronic components, a volume reduction of about 10% may be viewed as a significant accomplishment. The physical interpretation of these results may be conceived as follows. For fixed values of the wall heat flux, q_w, the smaller the Gr_L, the smaller the height of the channel L, for fixed values of b. Consequently, this gives rise to more pronounced diffusive effects. As already mentioned, these diffusive effects were not taken into account in ref. [2]. Besides, the authors imposed the pressure equal to the ambient one at both the inlet and exit of the channel.

In Fig. 6, where the modified nondimensional pressure drops along the centerline of the computational domain, at two Gr_L numbers and for several aspect ratios, are shown, the dramatic reduction of the pressure P_L, that takes place upwind of the channel inlet, can be seen. Therefore, we can convincingly conclude that the usage of the ambient pressure at the channel inlet, as well as at the channel exit, is an inaccurate hypothesis. More, it can be noted, as previously mentioned, that there is an increase in the pressure drops as the b/L decrease, i.e. as the channel gap is narrowed, for fixed L.

Table 1. Optimal values of the channel spacing

$(b/L)_{opt}$	Gr_L 10^2	10^3	10^4	10^5
Present work	1.90	1.20	0.78	0.51
ref. [2]	2.14	1.35	0.85	0.54
% Error	12.6	12.5	9.0	5.9

Alternatively, the idealization of either parabolic or uniform velocity profiles at the channel inlet can be incorrect or, at least, not very accurate for every value of the Grashof number. In fact, this aspect can be corroborated in Fig. 7, where the velocity profiles are drawn at different heights of the channel, for the four values of the Gr_L.

Figure 7 shows the evolution of the dimensionless velocity profiles at different channel heights with the four investigated Gr_L numbers, the aspect ratios being 1.9, 1.2, 0.8 and 0.5, i.e. close to the optimal values. These figures elucidate the fact that the inlet profile at $Gr_L = 10^2$ is closer to a parabolic one than a uniform one. In contrast, at $Gr_L = 10^5$ the velocity profile tends to a uniform one. This behaviour can be explained by the mere presence of the terms accounting for the momentum diffusion. In actuality, the disturbance produced by the plates of the channel diffuses upstream more vigorously as Gr_L diminishes, making the velocity profile less uniform.

Dimensionless temperature profiles across the channel spacing, at different heights and at the same four Gr_L numbers and the corresponding optimal b/L, are shown in Fig. 8. Here, it can be observed that as Gr_L diminishes, the temperature profiles at the channel inlet exhibit a temperature value where the core of the working fluid is nearly at the ambient temperature, viz. undisturbed. This is caused by the presence of the thermal diffusive effects that tend to decrease as Gr_L increases, i.e. as L is enlarged for a fixed channel gap b. Furthermore, the same diffusive thermal effects bring a reduction of the temperature close to the wall with respect to the immediately upstream section.

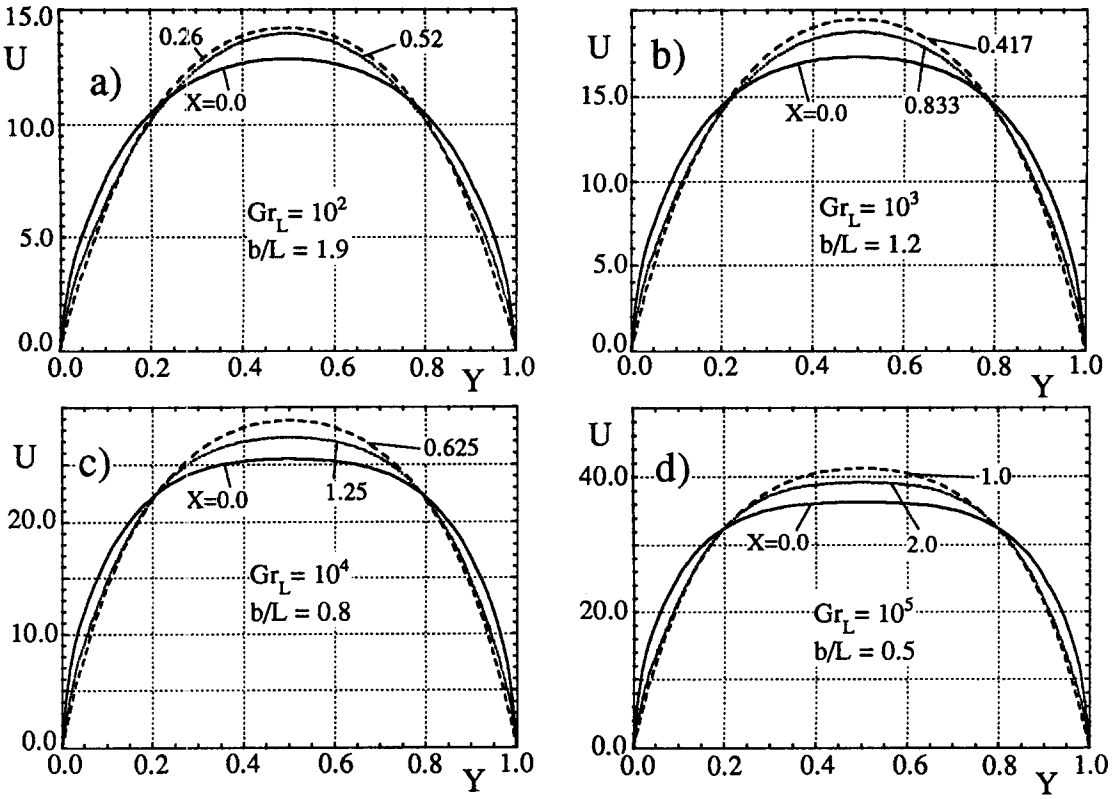

Fig. 7. Dimensionless velocity profiles as a function of the Y coordinate at different stations: (a) $Gr_L = 10^2$, $b/L = 1.9$; (b) $Gr_L = 10^3$, $b/L = 1.2$; (c) $Gr_L = 10^4$, $b/L = 0.8$; (d) $Gr_L = 10^5$, $b/L = 0.5$.

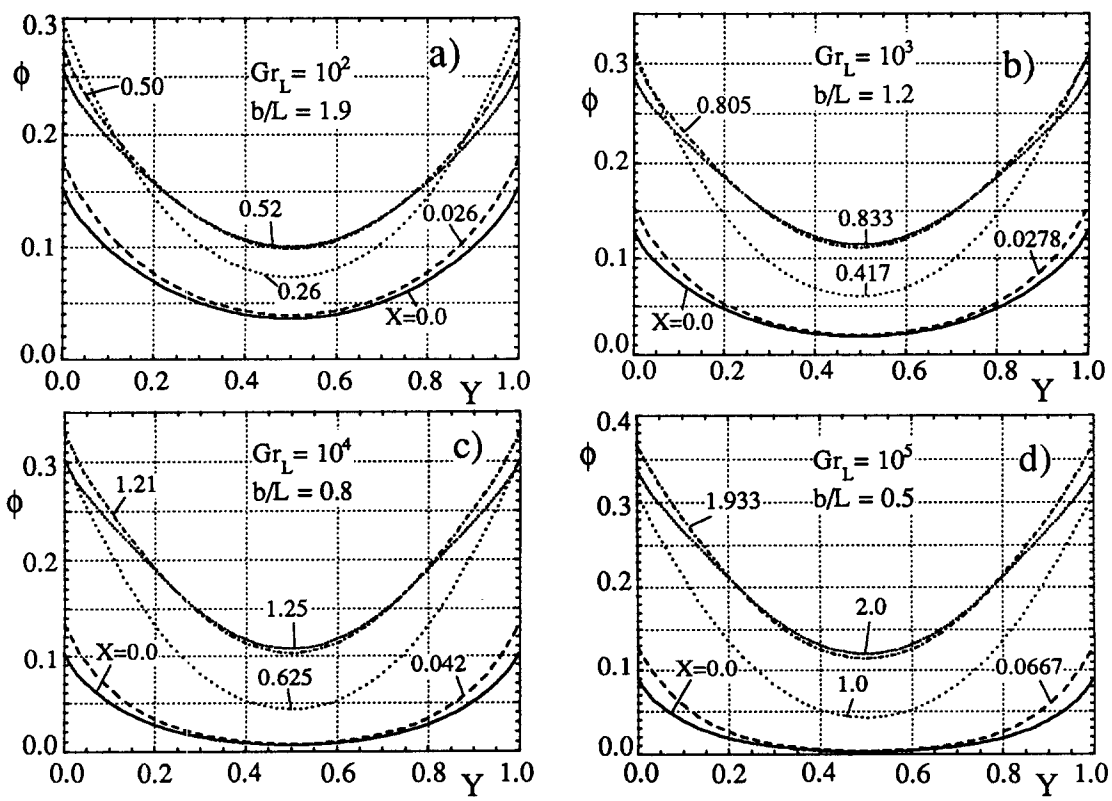

Fig. 8. Dimensionless temperature profiles as a function of the Y coordinate at different stations: (a) $Gr_L = 10^2$, $b/L = 1.9$; (b) $Gr_L = 10^3$, $b/L = 1.2$; (c) $Gr_L = 10^4$, $b/L = 0.8$; (d) $Gr_L = 10^5$, $b/L = 0.5$.

5. CONCLUSIONS

This paper reports results for the optimal aspect ratios of vertical, symmetrically heated channels, that are cooled by the upflow natural convection of air. Comparisons with a previous investigation show discrepancies in the optimal value of b/L, that are magnified as Gr_L diminishes. The magnitudes of the relative errors range from 12.6% at $Gr_L = 10^2$ to 6% at $Gr_L = 10^5$. The deviations at small values of Gr_L suggest that the momentum and thermal diffusive effects of the conservation equations are of paramount importance. This model necessitates enlarged, I-type computational domains. This is a realistic way to optimize the plate spacing of a single channel, from a thermal point of view. Correlations relating the induced mass flow rate as well as the optimal aspect ratio of the channel, b/L, with the thermo-geometrical parameters involved in this study have been proposed.

Acknowledgements—This work has been partially supported by a grant—MURST 40% 1993.

REFERENCES

1. Bar-Cohen, A. and Rohsenow, W. M., Thermally optimum spacing of vertical natural convection cooled, parallel plates. *ASME Journal of Heat Transfer*, 1984, **106,** 116–123.
2. Anand, N. K., Kim, S. H. and Fletcher, L. S., The effect of plate spacing of vertical, natural convection between heated parallel plates. *ASME Journal of Heat Transfer*, 1992, **114,** 515–518.
3. Bodoia, J. R. and Osterle, J. F., The development of free convection between heated vertical plates. *ASME Journal of Heat Transfer*, 1962, **84,** 40–44.
4. Levy, E. K., Optimum plate spacing for laminar natural convection heat transfer from parallel vertical isothermal flat plates. *ASME Journal of Heat Transfer*, 1971, **93,** 463–465.
5. Kettleborough, C. F., Transient laminar free convection between heated vertical plates including entrance effects. *International Journal of Heat & Mass Transfer*, 1972, **15,** 883–896.
6. Nakamura, H., Yutaka, A. and Naitou, T., Heat transfer by free convection between two parallel flat plates. *Numerical Heat Transfer*, 1982, **5,** 65–106.
7. Chang, B. and Lin, K., Transient buoyancy-induced flow through a heated, vertical channel of finite height. *Numerical Heat Transfer, Part A*, 1989, **16,** 15–35.
8. Naylor, D., Floryan, J. M. and Tarasuk, J. D., A numerical study of developing free convection between isothermal vertical plates. *ASME Journal of Heat Transfer*, 1991, **113,** 620–626.
9. Martin, L., Raithby, G. D. and Yovanovich, M. M., On the low Rayleigh number asymptote for natural convection through an isothermal, parallel-plate channel. *ASME Journal of Heat Transfer*, 1991, **113,** 899–905.
10. Shyy, W., Gingrich, W. K. and Gebarth, B., Adaptive grid solution for buoyancy-induced flow in vertical slots. *Numerical Heat Transfer, Part B*, 1992, **114,** 515–518.
11. Manca, O., Morrone, B. and Naso, V., A numerical study of natural convection between symmetrically heated vertical parallel plates. *Proceedings of the XII Congresso Nazionale sulla Trasmissione*, Vol. 1, Unione Italiana di Termofluidodinamica, 1994, pp. 379–390.
12. Torrance, K. E., *Handbook of Heat Transfer—Fundamentals*, 2nd edn, Chap. 5. McGraw–Hill, New York, 1985.
13. Roache, J. P., *Computational Fluid Dynamics*. Hermosa, Albuquerque, NM, 1972.